SINET: Ethiop. J. Sci., 24(1):51–68, 2001
 ISSN: 0379–2897

SURFACE KINETIC TEMPERATURE MAPPING USING SATELLITE SPECTRAL DATA IN CENTRAL MAIN ETHIOPIAN RIFT AND ADJACENT HIGHLANDS

Tenalem Ayenew

Department of Geology and Geophysics, Faculty of Science, Addis Ababa University
PO Box 1176, Addis Ababa, Ethiopia, E-mail: dgg@telecom.net.et

ABSTRACT: Remotely sensed thermal-infrared spectral data can be used to derive surface temperature of any object if the optical and thermal properties are known. In this study TM band six has been used to assess the spatial variability of the kinetic temperature of the central Ethiopian rift lakes and adjacent highlands. NOAA-AVHRR data have been used to understand the relative differences of the monthly lake surface kinetic temperatures. The result revealed that despite the limited topographic differences of the rift lakes and their proximity, the surface kinetic temperature difference is high, mainly due to groundwater and surface water fluxes. From thermal signature analysis two hot springs below the lake bed of Ziway were discovered. The various hot springs around three of the lakes have limited role in the overall water budget of these lakes as compared to the total surface water and cold groundwater fluxes. Temperature from the land surface shows also large variations with altitude and land cover types.

Key words/phrases: Kinetic temperature, rift lakes, spectral data, thematic mapper, thermal infra-red

INTRODUCTION

One of the first uses of thermal images in hydrogeology is to detect temperature contrasts due to up-welling groundwater in water bodies using Thematic Mapper (TM) data (Meijerink; 1996). In some later studies, such contrasts are associated with groundwater discharge areas (Bobba *et al.*, 1992; Batelaan *et al.*, 1993; Tenalem Ayenew, 1998). Short-wave thermal infra-red data have also been used

to discover high temperature thermal events and for geothermal resources assessment (Rothery *et al.*, 1988).

The use of thermal infra-red data is becoming increasingly useful for measuring different surface flux densities and temperatures (Menenti, 1984; Bastiaanssen, 1995; Pelgrum and Bastiaanssen, 1996). Lagouarde (1991) suggests the possibility of using the National Oceanic and Atmospheric Administration (NOAA) Advanced Very High Resolution Radiometer (AVHRR) for a radiation balance. He proposed a simple algorithm for estimating the upward long-wave component of the surface radiation balance from only one surface measurement derived from NOAA. TM and NOAA-AVHRR have also been used for evapotranspiration mapping (Kerr *et al.*, 1992, Parodi, 1993; Timmermans, 1995; Tenalem Ayenew, 1998).

Cloud free multi-temporal spectral data of TM and NOAA can be of great help in assessing the temporal variation of temperature and evapotranspiration from the land and water bodies (Parodi, 1993). However, due to the high cost of TM images, its application in multi-temporal analysis of hydrometeorlogical process is very limited.

In this study, thermal infra-red TM band 6 data of a single scene were used for different purposes. Temperature contrasts in the lakes are of interest in the area to detect whether hydrothermal activities occur and if so, the relative importance of the discharges. Hydrothermal water could also influence the temperature of river water discharging into the lakes.

A second application is to assess the differences in temperature of the lakes, which are associated with different evaporation rates. Since there are no field data available on lake evaporation, ancillary information for this important factor of the water budget is useful. In this connection, in addition to TM, the NOAA-AVHRR data was used to derive the mean monthly surface kinetic temperatures of the lakes using cloud free images at the National Meteorological Services Agency.

The third application is to study the geothermal manifestations in relation to the rift geologic structures; the study area is characterized by many hot springs and fumaroles associated with geothermal fields. This helps to detect possible

migration routes of groundwater. Spring discharges emanating below the lakes could also be estimated from thermal images.

The TM image was taken on 21 November 1989 (satellite overpass at 10:00 AM local time). TM band six operates between the wave length range of 10.4 μm and 12.5 μm of the thermal infra-red region with a ground resolution of 120 m. For monthly lake surface temperature estimation, the NOAA-AVHRR data (1994–1995) were used based on the method described by Bastiaanssen (1995). It acquires images with a swath width of 2,700 km and a ground resolution of 1,100 by 1,100 metres. The raw TM spectral data were converted to surface kinetic temperature by image processing techniques using the Integrated Land and Water Information System (ILWIS) software developed at the International Institute for Aerospace Survey and Earth Sciences (ITC), The Netherlands.

THE STUDY AREA

The basin studied is part of the Ethiopian Rift system bounded within the limits of 38°00'-39°30' east longitude and 7°00'–8°30' north latitude, and covers a total area of 13,000 km^2 of which 1,265 km^2 is permanent open water body. The central part is the floor of the rift occupied by four major lakes: Ziway, Langano, Abiyata and Shala, having average depths of 2.4, 21.9, 8.9 and 8.6 metres respectively (Table 1). Shala and Abiyata are highly alkaline terminal lakes with no surface water outlets fed by perennial rivers coming from the eastern and western highlands (Fig. 1). Hot springs emanating from the southern, southeastern and eastern shores feed Shala, Langano from springs located on the northern shore and in one of the northern islands. A low discharge hot spring exists in one of the southern islands of Ziway. Fig. 1 shows the main sites of geothermal manifestations.

The altitude ranges from a little over 3,000 meters above mean sea level (m.a.s.l) in large part of the surface water divide to 1,600 m.a.s.l around the rift lakes. The average altitude of the rift is about 1,700 m.a.s.l. The altitude ranges from 2,000 to 3,000 m.a.s.l in the western highland and 2,100 to 3,200 m.a.s.l in the eastern highlands. There are volcanic summits having an altitude of more than 4,000 m.a.s.l to the east (Tesfaye Chernet, 1982).

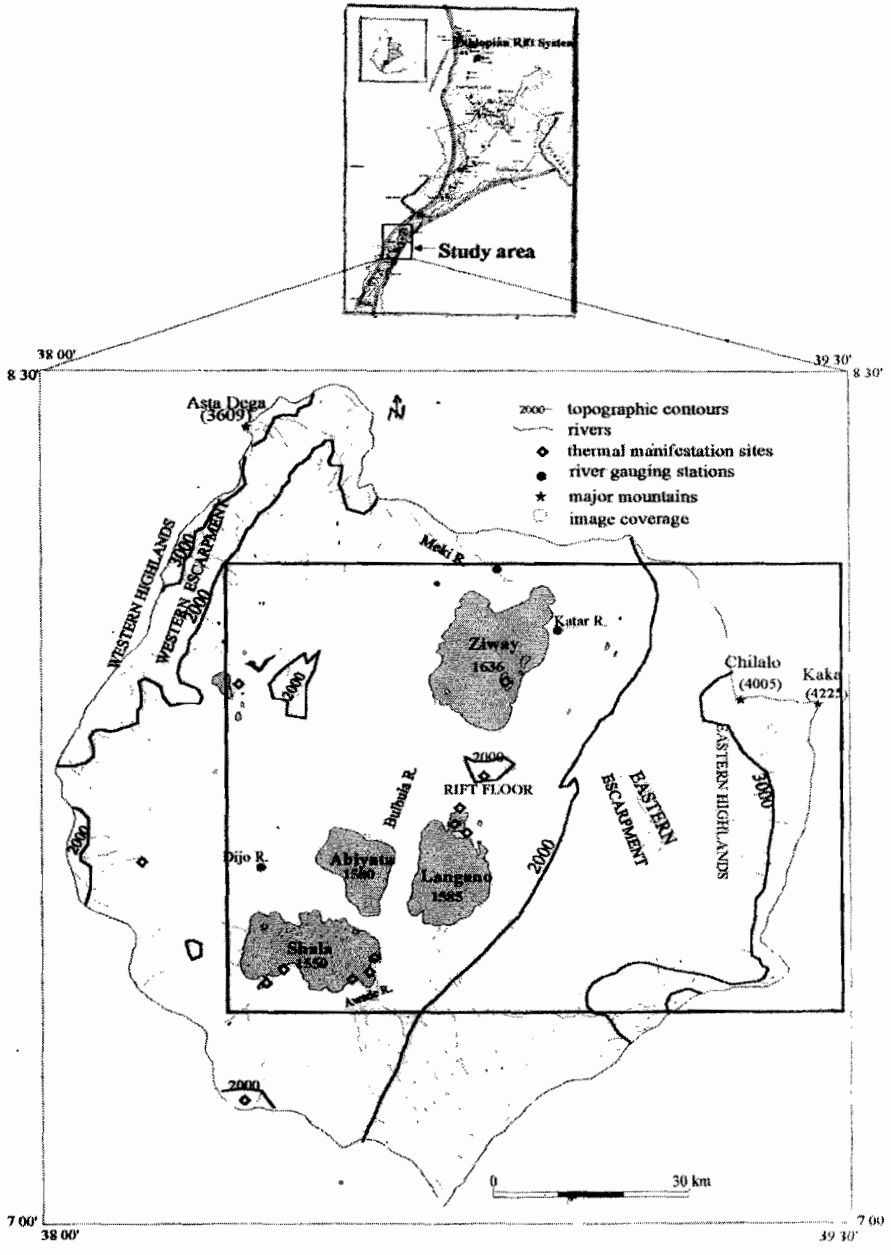

Fig. 1. Location map of the study area.

Geologically these lakes are situated in tectonically active rift volcanic terrain. The present day geologic and geomorphic features are the result of Cenozoic volcano-tectonic and sedimentation processes. Faulting was accompanied by extensive basaltic and silicic volcanism restricted to separate centres aligned along the NE-SW trending rift axis. Several shield volcanoes were developed in the plateaux; the different volcanic episodes formed thick rock sequences (Di Paola, 1972; Giday Woldegebriel *et al*, 1990). The major rock types in the rift are: ignimbrite, basalt, tuff, trachyte and pumice, associated with lacustrine, volcano-clastic, alluvial and colluvial deposits. Large-scale block faulting has disrupted these rocks and formed step-faults. As a result, the rift is distinctly separated from the highlands by a series of normal faults mainly trending parallel and sub-parallel to the axis of the rift. The floor of the rift is marked by a persistent belt of intense and active faulting and volcanic centres characterized by presence of hot springs and fumaroles.

The climate is humid to sub-humid in the highlands and semi-arid in the rift. Mean annual temperature is about 15°C in the highlands and around 20°C in the rift (HALCROW, 1989). The average annual rainfall ranges from about 1,150 mm in the eastern and western highlands to around 650 mm in the rift floor. At the top of large volcanic summits the annual rainfall can be as high as 1400 mm (Tenalem Ayenew, 1998). The main rainy season is between June and September. The dry season lasts from October to February. Temperature and rainfall show strong altitudinal variations (Tesfaye Chernet, 1982).

Most of the basin is moderately cultivated and, in major mountainous areas there is no much agriculture due to topographic and climatic constraints. Afro-montane forest lies between 2,000 and 3,000 m.a.s.l, above which alti-montane vegetation is found. The top of mountains is covered by afro-alpine vegetation. The escarpment is characterized by acacia and deciduous trees, evergreen and semi-evergreen bush land. On the southeastern escarpment large forested area exists (represented by black tone in Fig. 2). The remaining highland and escarpment is farmland with scattered trees and grazing land. Except few irrigated fields around lake Ziway, the rift is covered by grass, bushes and shrubs. Soda grounds and lacustrine soils in the rift floor are represented by strong white tone in Fig. 2. Table 2 shows the land cover types derived from multi-spectral classification of TM bands 2,3 and 4.

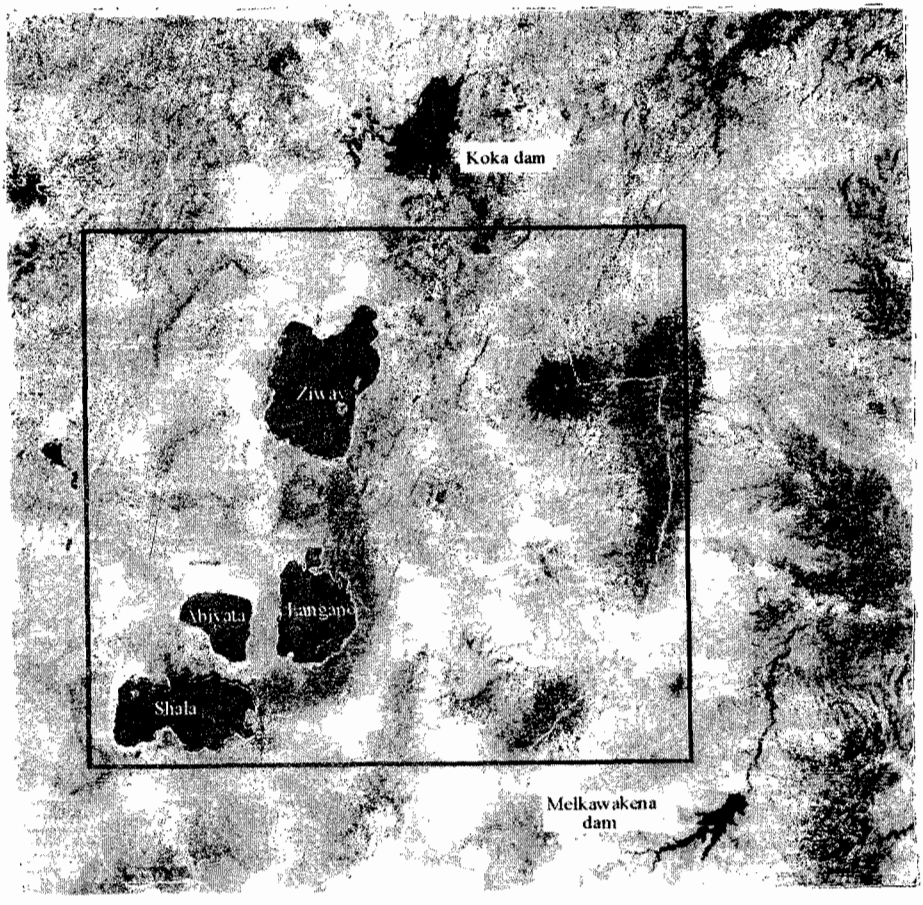

Fig. 2. Panchromatic TM image showing part of the basin and adjacent areas. The white line is the surface water divide of the basin. The thick black line indicate the scene chosen for the analysis.

Table 1. Basic hydrologic data of the major lakes (modified from HALCROW, 1989).

Lake	Altitude (m.a.s.l)	Lake area (km^2)	Catchment area (km^2)	Maximum depth (m)	Mean depth (m)	Volume (mcm)
Abiyata	1580	180	10740	14.2	7.6	954
Langano	1585	230	2000	47.9	17	3800
Shala	1550	370	2300	266	8.6	37000
Ziway	1636	440	7380	8.9	2.5	1466

Table 2. Areal coverage of land cover units in the basin.

Class	Land cover types	Areal coverage (%)	Area (km^2)
1	Permanent open water body	11.1	1443
2	Marshy areas, swamps and seasonal ponds	1.4	182
3	irrigated agricultural fields	0.7	91
4	large-scale rain-fed agriculture	1.2	156
5	pasture and farm plots with scattered trees and orchards	66.1	8593
6	dominantly grassland	3.6	468
7	bushes, shrubs and grassland with rare farm plots	7.3	949
8	woodland and afro-alpine vegetation	8.4	1092
9	settlement areas	0.2	26

METHODOLOGY

The radiant temperature of a given surface can be derived from the TM band 6 pixel values or digital number (DN) using the following relation developed by Markham and Barker (1986).

$$L_i = L_{\min,i} + \frac{L_{\max,i} - L_{\min,i}}{DN_{\max}} \cdot DN \qquad (1)$$

where, Li : spectral radiance in band i ($mW/cm^2.str.\mu m$)
$L_{min,i}$: spectral radiance at DN = 0 ($mW/cm^2.str.\mu m$)
$L_{max,i}$: spectral radiance at DN = max ($mW/cm^2.str.\mu m$)
DN : digital number
DN_{max} : grey level for the analyzed pixel

Once the spectral radiance is computed, it is possible to calculate the radiant temperature using the relation:

$$T_R = \frac{K_2}{\ln(\frac{K_1}{L_1} + 1)} \quad (2)$$

where, TR : radiant temperature (°K)
K_1 : calibration constant (60.776 mW/cm^2.str.μm)
K_2 : calibration constant (1260.56 mW/cm^2.str.μm, °K)
L_i : spectral radiance in band i (mW/cm^2/str/μm)

From the radiant temperature the kinetic temperature (T_{toa}) at the top of the atmosphere can be calculated by:

$$T_{toa} = \varepsilon^{0.25} T_R \quad (3)$$

The ε term represents the spectral emissivity. Since the emissivity of pure water is 1, the relation between the recorded signal at the satellite and the relative surface water temperature is a simple one. However, for conversion to absolute temperature, the effect of the atmosphere has to be accounted for. For land surfaces the interpretation of thermal imagery is not so simple, because the emissivity of the various land covers vary in a wide range due to variable thermal properties of soil-vegetation complexes. Topographic conditions, which determine slope exposure in relation to the sun's path prior to satellite overpass, also play a role.

A simplified approach to estimate the emissivity of the land using Normalized Difference Vegetation Index (NDVI) suggested by Griend *et al.* (1993) is

$$\varepsilon = 1.009 + 0.047 \ln(\text{NDVI}). \quad (4)$$

The above relation does not give the actual land surface temperature. It has to be converted to surface kinetic temperature (T_o) after corrections for atmospheric effects (Roerink, 1995). The general relation is given by:

$$T_o = \sqrt[4]{\frac{\sigma T_o^{R4} - (1-\varepsilon) L^{\downarrow}}{\sigma \varepsilon}} \quad (5)$$

Where, TR : black body surface temperature (°K)

$L^{\downarrow}$: incoming long-wave radiation derived from spectral data (W/m^2)

σ : Stefan Boltzman constant (5.6697×10^{-8} $W.m^{-2}$. K^{-4})

RESULTS AND DISCUSSION

Figure 3 shows the classified surface kinetic temperature of the lakes and the surrounding landscape established after appropriate atmospheric corrections. Table 3 shows the instantaneous surface kinetic temperature of the lakes derived from TM. The monthly surface temperature of the lakes derived from NOAA is given in Table 4.

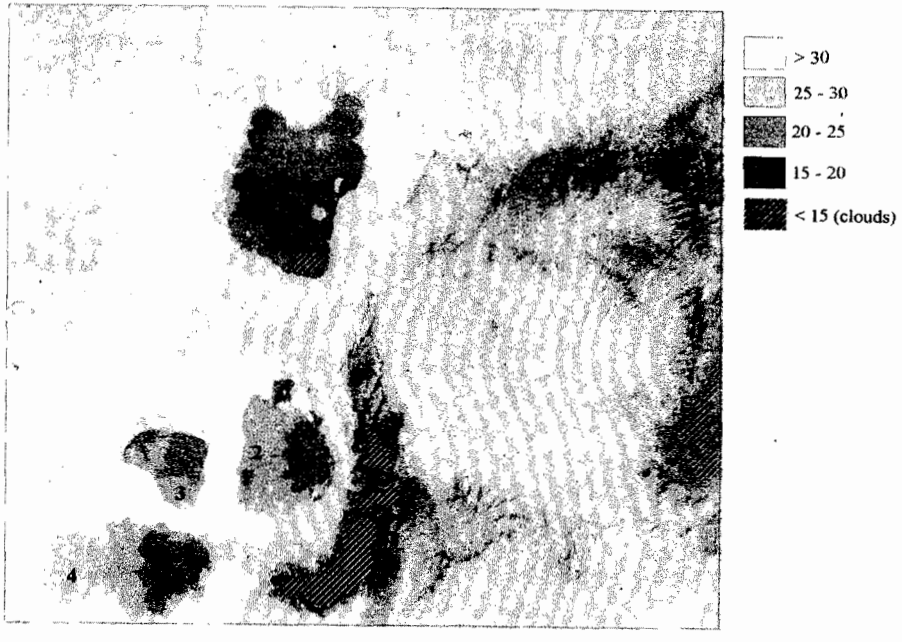

Fig. 3. Classified TM band six image showing surface kinetic temperature (°C) (1, Lake Ziway; 2, Lake Langano; 3, Lake Abiyata; 4, Lake Shala).

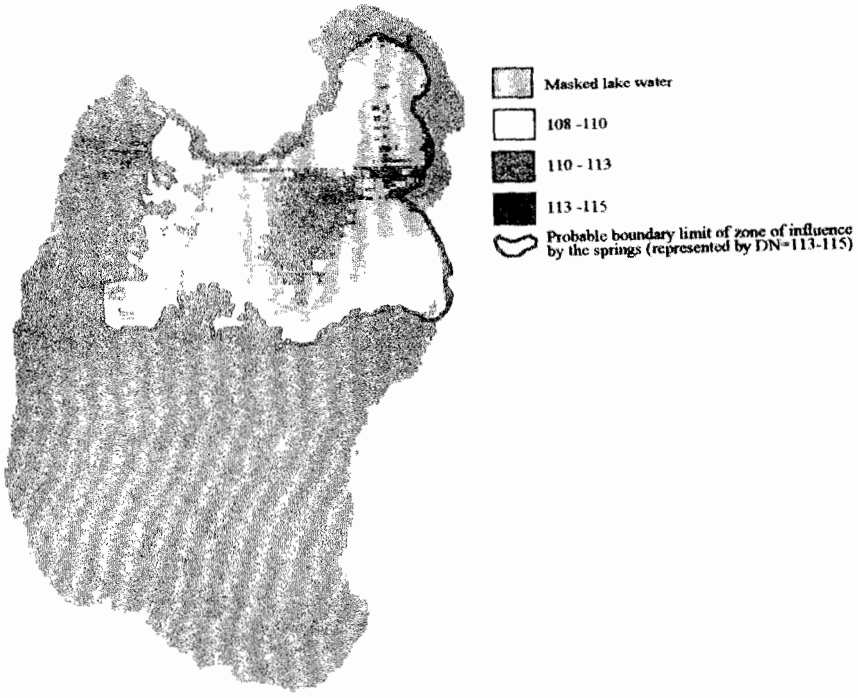

Fig. 4. Sites of hot spring emanation inside Lake Ziway (the highest DN value).

Table 3. Lake surface kinetic temperature (°C).

Basic statistics	Abiyata	Langano	Shala	Ziway
Average	22.9	22.5	23.2	20.9
Minimum	19.0	15.4	16.2	16.2
Maximum	27.4	27.0	26.9	26.8
Mode	20.9	21.8	22.7	20.4
St. deviation	0.9	1.1	1.2	0.9

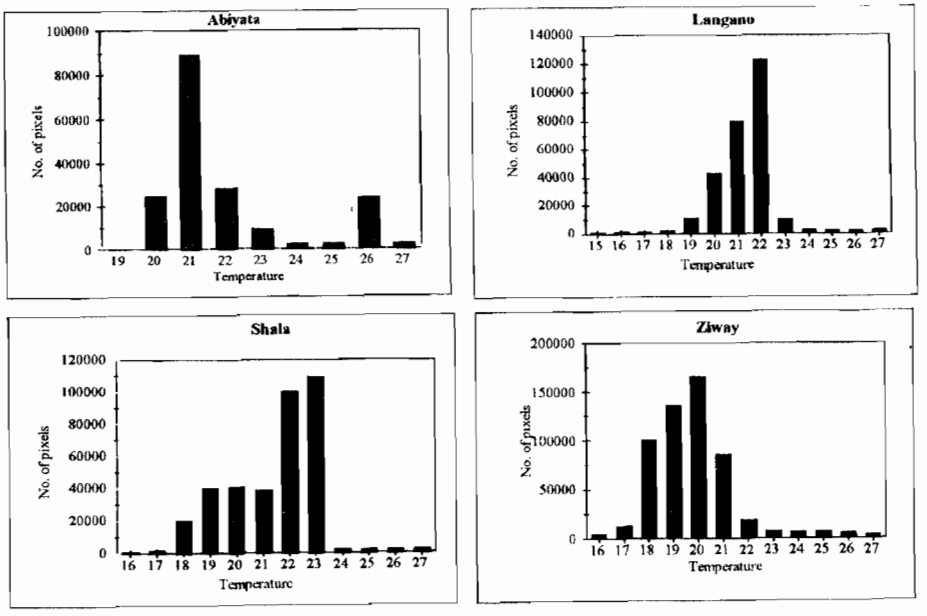

Fig. 5. Histograms of surface kinetic temperature of the lakes (°C).

Table 4. Surface temperature of the lakes derived from NOAA (°C). (min, minimum; avg, average; max, maximum.)

Lake		Jan	Feb	Mar	Apr	May	Jun	Jul	Aug	Sep	Oct	Nov	Dec
Ziway	min		17.8	15.6	16.8	21	18.6	17.6	17.8		18.2	19.2	19.6
	avg		18.4	18.8	23.2	23	20.6	19.2	18.4		20.4	22.6	23.2
	max		22	29.2	32	37	31	29.2	22		35.4	35.4	44.6
Langano	min		12.2	17	20.2	21.6	19.2	15.6	12.2		19	20.4	21.4
	avg		20	20.2	21.8	23.8	22	19.8	20		22.2	24.8	24.8
	max		22.6	29	29.8	33.8	31.8	29.2	22.6		33.6	37	40.4
Abiyata	min		13.8	16	20.4	22	16.6	17.2	13.8		19.2	20.2	20
	avg		19	20.8	22.6	25.4	21.2	20.6	19		22.8	26.6	25.4
	max		22.2	26.6	28.4	7.4	32.2	30	22.2		36.4	39.2	41
Shala	min		16.8	16	19.6	1.4	12.8	16.4	16.8		19	20.4	20.4
	avg		18.8	19.2	20.8	23	20.6	18.6	18.8		22	23.4	22.6
	max		21.8	24.8	26.8	32.2	30.8	23.6	21.8		34.2	34.8	32.2

Lake surface temperature

The result shows wide variation in the surface temperature of the lakes. This variation has resulted in large differences in the rates of open-water evaporation (Tenalem Ayenew, 1998). As illustrated in Fig. 3, not all the lakes have a uniform surface temperature. The lowest value usually exists far from the shores in the central and deeper part of the lakes. Locally this pattern is disrupted by the effect of inflowing rivers and groundwater fluxes. For example, there is a lower temperature at the confluence of Meki river with lake Ziway, and the rivers of Horakelo and Bulbula with lake Abiyata. Low temperature signature is evident close to the eastern shore where large rivers enter into lake Langano. These low temperature sites close to shores are also localities of large groundwater inflow; as identified from groundwater flow models simulations (Tenalem Ayenew, 2001).

The effect of the Katar river which comes from the eastern highlands entering lake Ziway from the northeastern side is not as important as the rivers coming to lakes Langano and Abiyata in affecting the temperature signature. Katar supplies the largest volume of cold water to lake Ziway. A large portion of the lake close to the confluence is very shallow; in the field it was found that there is no indication of geothermal manifestations around the lake. However, the hot springs emanating below the lake bed, a little south of the confluence (Fig. 4), might play a role in raising the temperature. Probably, the huge sediment of the mouth of the Katar delta at the confluence may reduce the water depth and consequently increase the surface temperature slightly.

The effect of known hot springs (Fig. 1) emanating close to shores on lake water temperature is not well pronounced. Although the points of emergence of hot springs is represented in local high temperature pixels to the south, southeast and east of lake Shala and north of lake Langano, there is little influence on the surface temperature. Lake surface temperature measurement was made in the field in these areas. There is only a rise of 1 to 2 °C from the normal colder lake water. This influence extends only up to a maximum of 20 to 30 meters far from the shores where these hot springs enter. In the presence of large hot spring fluxes, the rise in temperature would have been much higher. This implies that the role of these hot springs is small in terms of volume of water compared to the contribution of water from rivers and cold

groundwater system. Some hot springs are masked by the presence of local clouds, as in the case of south Ziway and the island in northern Langano. Some springs north of Langano are also masked by the presence of dense big trees.

From the histograms of kinetic temperature of the lakes (Fig. 5), the following generalizations can be made:

On the average, Abiyata and Shala have the highest surface temperature. In lake Abiyata the lower temperature of the histogram (19–21°C) is related to areas where rivers Bulbula and Horakelo enter into the lake from the north (Fig. 1), and the highest temperature distribution is related to areas in the southern tip and northern shallow part of the lake. The large number of pixels around 26°C refers to the southern tip and northern side of the lake where the water is extremely shallow. The shoreline in these areas is covered with white soda salts with very high temperature signature.

In lake Shala the lowest temperature corresponds to the deepest part of the lake and the small cloud covered areas (represented in less than 15°C in Fig. 3). The effect of the rivers coming from the southeastern highlands is represented by low temperature in the eastern half of the lake. The Dijo river, which comes from the western highlands into the lake, does not have a visible influence on temperature of the lake. This is due to upstream diversion of the river for irrigation. In Langano the lowest temperature (less than 19°C) is measured in the northern part around the island. The cloud cover areas are less than 15°C in Fig. 3. Very local highest temperature points are present on the northern shore where hot springs emanate. The 22–25°C value represents lake water influenced by incoming cold rivers.

Lake Ziway has the lowest temperature. This is partly related to the large quantity of cold water that comes from the two major rivers. High surface temperature exists close to the shallowest parts in the western and southern side where there are no inflowing rivers. Areas close to the small islands are represented by higher temperatures (25–27°C). This is probably due to the thermal exchange between the volcanic rocks and the lake water.

Geothermal fields and hydrothermal activities

A simple threshold value of the digital data allows discrimination of higher thermal signatures than the rest of the land. In this case the lowest kinetic temperature for geothermal manifestations on the land is 30°C. Although local geothermal manifestations are not clearly visible from the thermal images, in general they are aligned along active faults and recent central volcanic complexes. The soda salts around lakes Abiyata and Shala have also high temperatures. Not all regional faults are associated with geothermal fields. For example, the active regional faults of the eastern and western escarpment are devoid of geothermal manifestations or high temperature signatures. The most important geothermal fields are localized around and close to the Shala caldera and the northern shore of Langano. These are due to the presence of local active volcanic centres.

The NOAA image has little practical importance in showing local high temperature grounds due to the low resolution. Some high temperature grounds and associated hot springs were not detected also from the high resolution TM image due to forest cover. In such kind of terrain thermal signature analysis requires careful field investigations. Many hot springs, which are not observable from the satellite data, were identified in the field.

Inside lake Ziway, not far from the confluence with Katar river, there are sites of high DN value (Fig. 4). The thermal signature analysis allowed to discover at least two hot springs emanating below the bed of lake Ziway. The hot pixels inside lake Ziway have a surface temperature of 2 to 4°C greater than the surrounding colder lake water (with average temperature of around 22°C). The discharge of these springs were found to be low (Tenalem Ayenew and Gieske, 2001).

Land surface kinetic temperature

The classified image shows that there is a large temperature difference between the rift and the highlands; the zonation of temperature with altitude is locally disrupted by clouds. The dominant instantaneous kinetic temperature for most of the rift valley ranges from 26°C to 30°C. The temperature reaches locally more than 35°C in geothermal fields. In the highlands, the temperature ranges from a little above 15°C in high volcanic summits to 28°C in the rift plains.

The land cover types also have important influence on land surface kinetic temperature. For example, the rift floor lacustrine bare soil surface has high temperature compared to the grasslands and bush lands. The effect of land use on temperature is better represented in the rift. Whenever bare soil is present, the temperature is greater than the nearby land covered with crops or trees. The contrast is very high between forested land and bare soil; there is on average 5°C to 8°C difference between the acacia trees cover (around 21°C) and nearby lacustrine soils (more than 28°C). The soda salts around lake Abiyata have a very high temperature (around 30°C). As in the case of the lakes, the large differences in temperature resulted in wide variations in evapotranspiration from the land surface.

CONCLUSIONS AND RECOMMENDATIONS

The thermal signature analysis has demonstrated its importance in showing the relative spatial differences in temperature under data scarce conditions and has served as source of ancillary information in the process of actual evapotranspiration estimation and water balance study of the rift lakes. However, the instantaneous temperature value obtained from TM may not be good enough to show the long-term variability. The high cost of TM images limited its application for the study of temporal variations of temperature in this case. But, the NOAA-AVHRR allowed an estimate of a range of values of the monthly lake surface temperature. The relative differences of NOAA-derived lake surface temperatures agree with the results obtained from TM band 6.

In this study more confidence can be placed on lake surface temperature than the surrounding landscape, since the physical factors involved in lakes are easier to estimate using satellite spectral data than those for heterogeneous land surfaces.

Conventional open-water evaporation estimation methods usually assume that the surface temperature of lakes remains uniform and that evaporation proceeds more or less at the same rate over the total lake surface. However, this study clearly demonstrated that temperature varies widely depending on surface temperature and reflectance, and on the incoming fluxes from groundwater and

surface waters. The remote sensing approach helps to refine the results obtained from conventional open water simulations.

The result has revealed that with high resolution cloud free multi-temporal images and limited ground data; areal temperature can be estimated using thermal infra-red spectral data. This has important implications in future water resources studies in East African rift lakes associated with geothermal fields. The discovery of hot springs below the lake using the TM image has important implications in lake water balance studies.

Both the field measurements and the remotely sensed data in this study show that the most alkaline lake of Abiayta and Shala are hotter. Abiyata has a higher surface temperature than Shala, though they have comparable alkalinity, albido and located close to each other. This may be related to its shallow depth and the thermal properties of lake water and bottom sediments and the influence of the surrounding soda grounds. Ziway has the lowest temperature due to its relatively larger volume and the large contribution of cold fresh water from the two major feeder rivers of the basin.

Temperature from the land surface shows also large variations. This is due to the difference in altitude and land cover types. Generally forested areas have lower temperature than bare grounds. The highest temperature has been observed in rift soda grounds and local thermal manifestation areas.

With bathymetric maps of the lakes, better spatial temperature variations can be assessed in relation to depth. Temperature readings with depth is very important to discover more hot springs in deeper parts of the lakes which cannot be discriminated easily from thermal signature analysis using thermal infra-red images.

In areas where large groundwater enters into the lakes, the surface temperature is quite low. With seepage meter observations in the lake beds, better relation can be constructed between groundwater flux and surface temperature signatures. This method can be used to determine groundwater inflow sites from satellite observations in other large rift valley lakes.

ACKNOWLEDGEMENTS

The author is very grateful to Ato Tuffa Dinku and the staff of the Remote Sensing Laboratory of the National Meteorological Services Agency for providing the NOAA image to derive monthly lake temperature. The author would like to extend his appreciation to the Department of Geology and Geophysics, Addis Ababa University for providing logistic support for field checks.

REFERENCES

1. Bastiaanssen, W.G.M. (1995). Regionalisation of surface flux densities and moisture indicators in composite terrain. A remote sensing approach under clear skies in Mediterranean climates. Agricultural University of Wageningen. PhD Thesis, The Netherlands, 273 pp.
2. Bobba, A.G., Bukata, R.P. and Jerome, J.H. (1992). Digitally processed satellite data as a tool in detecting potential groundwater flow systems. *Journal of Hydrology* **131**:25–62.
3. Batelaan, O., de Smedt, F. and Otero Valle, M.N. (1993). Development and application of a groundwater model integrated in the GIS GRASS. **In:** *HydroGIS 93, International Association of Hydrological Sciences Publ.* no. 211, pp. 581–589.
4. Di Paola, G.M. (1972). The Ethiopian Rift Valley (between 7°00⅔ and 8°40⅔ Lat. North). *Bull. Volcanol.* **36**:517–560.
5. Giday Woldegebriel, Aronson, J.L. and Walter, R.C. (1990). Geology, geochronology, and rift basin development in central sector of the Main Ethiopian Rift. *Geol. Soc. Amer. Bull.* **102**:439–458.
6. Griend, A., Van de, A. and Owe, M. (1993). On the relationship between thermal emissivity and normalized difference vegetation index for natural surfaces. *J. Rem. Sens.*, **14**:1119–1131.
7. HALCROW (1989). Rift valley lakes integrated natural resources development master plan. Ethiopian Valleys Development Studies Authority, Unpub. Report, Addis Ababa, Ethiopia.
8. Kerr, Y.H., Lagourade, J.P. and Imbernon, J. (1992). Accurate land surface temperature retrieval from AVHRR data with use of an improved split–window algorithm. *Remote Sensing of the Environment* **41**:197–209.
9. Lagourade, J.P. (1991). Use of NOAA-AVHRR data combined with agrometeorological model for evapotranspiration monitoring. *J. Rem. Sens.* **12**:1853–1854.

10. Markham, B.L. and Barker, J.L. (1986). Landsat MSS and TM post-calibration dynamic ranges, exoatmospheric reflectance at satellite temperatures. EOSAT Landsat Technical Note 1. (new look-up tables), August 1986.

11. Meijerink, A.M.J. (1996). Remote sensing applications to hydrology: Groundwater. *J. Hydrol. Sci.* **41**(4):549–561.

12. Menenti, M. (1984). Physical aspects and determination of evaporation in deserts, applying remote sensing techniques. PhD Thesis, Wageningen Agr. Univ., ICW Publ. Wageningen. The Netherlands, 184 pp.

13. Parodi, G.N. (1993). An up to date inventory of remote sensing potentiality in the energy balance equation approach for actual evapotranspiration mapping. Basic theory and prospects. MSc thesis. ITC, Enschede, The Netherlands, 94 pp.

14. Pelgrum, J. and Bastiaanssen, W.G.M. (1996). An intercomparison of techniques to determine the area averaged latent heat flux from individual *in situ* observations: A remote sensing approach using the European field experiment in desertification-threatened area data. *Water Resources Research* **32**(9):2775–2786.

15. Roerink, G.J. (1995). SEBAL estimations of the areal patterns of sensible and latent heat fluxes over the HAPEX Sahel grid, Interne Mededling 364, DLO-Staring Centre, Wageningen, The Netherlands.

16. Rothery, D.A., Francis, P.W. and Wood, C.A. (1988). Volcano monitoring using short wavelength infrared data from satellite. *J. Geophys. Res.* **93**:7993–8008.

17. Tenalem Ayenew (1998). The hydrogeological system of the lake district basin, Central Main Ethiopian Rift. PhD Thesis, Free University of Amsterdam, The Netherlands, 259 pp.

18. Tenalem Ayenew and Gieske A.S.M. (2001). Determination of hot spring discharge in Lake Ziway (Ethiopia) by remote sensing. *ITC Journal*, (in press).

19. Tenalem Ayenew (2001). Numerical groundwater flow modelling of the Central Main Ethiopian Rift lakes basin, SINET: *Ethiop. J. Sci.* (in press).

20. Tesfaye Chernet (1982). Hydrogeology of the Lake Region, Ethiopia. Ethiopian Institute of Geological Surveys, Addis Ababa, Memoir N° 7.2

21. Timmermans, W. (1995). Remote sensing evapotranspiration. MSc thesis, Delft University of Technology. Delft, The Netherlands, 153 pp.